A theoretical and experimental study of the distorted pyrochlore $Bi_2Sn_2O_7$

Aron Walsh,[a] Graeme W. Watson,*[a] David J. Payne,[b] Gregory Atkinson[b] and Russell G. Egdell[b]

Received 5th May 2006, Accepted 12th July 2006
First published as an Advance Article on the web 27th July 2006
DOI: 10.1039/b606413b

The pyrochlore based bismuth stannate, $Bi_2Sn_2O_7$, is a material with important applications in catalysis and gas sensing. The thermodynamically stable α phase has 352 atoms in the unit cell and is one of the most complex oxide crystal structures to have been solved by powder diffraction. We have performed a full atomic relaxation and calculated the electronic structure, using gradient corrected density functional theory, with the resulting structure in very good agreement with the previous experimentally determined unit cell. The computed density of states is in excellent agreement with our valence band X-ray photoelectron spectra. The combined results shed new light on the bonding and lone pair activity in this material. A mixture of Bi 6s and O 2p states are found to dominate the top of the valence band while Sn 5s, O 2p and Bi 6p states dominate the bottom of the conduction band. The differing contributions of Sn 5s and Bi 6s states to the valence and conduction bands reflect both differences in atomic binding energies and differences in the strength of the metal s interactions with O 2p. The preference of this material for a distorted structure and its unique catalytic and gas sensing activity are discussed.

1. Introduction

$Bi_2Sn_2O_7$ is of considerable interest due to its catalytic activity in a number of processes including the oxidation of hydrocarbons[1] and the partial oxidation of isobutene.[2] In addition, it can also act as a gas sensor with selectivity toward CO.[3,4] While lanthanide tin oxide adopts the regular cubic pyrochlore structure, $Bi_2Sn_2O_7$ does not, but instead exists as a number of polymorphs.[5] α-$Bi_2Sn_2O_7$ is the thermodynamically stable phase at room temperature, whose monoclinic ($\beta = 90.038^\circ$) crystal structure was only recently determined.[6] With 352 atoms in the unit cell, it is one of the most complex oxide structures to have been solved by powder diffraction, Fig. 1. The structure is a deformed supercell of the cubic pyrochlore lattice in which the Bi atoms have distorted away from their ideal positions. In the temperature range between 130 °C and 630 °C face centred cubic β-$Bi_2Sn_2O_7$ becomes favoured. Finally above 630 °C the cubic pyrochlore based γ phase is adopted.

In $Bi_2Sn_2O_7$, Sn is formally considered to adopt a +4 oxidation state giving it an electronic configuration of $4d^{10}5s^0$. Bi adopts its +3 oxidation state giving it an electronic configuration of $5d^{10}6s^2$. The Bi(III) oxidation state is commonly associated with low symmetry crystal structures which are rationalised in terms of stereochemically active lone pairs formed by hybridisation of Bi 6s states with Bi 6p. The distorted pyrochlore structure of $Bi_2Sn_2O_7$ which is favoured over the higher symmetry cubic structure is a typical example of this effect. The lone pairs have also been suggested as being important in catalytic oxidation processes.[7]

We have recently performed a series of computational and experimental studies on lone pair activity in heavy metal oxides[8–15] which show that lone pairs in these materials do not conform to the classical ns^2 model. Filled antibonding cation s and anion p states are the source of the asymmetry in the electron density. As such the role of the Bi 6s electrons in $Bi_2Sn_2O_7$ may be more complicated than simple classical considerations would suggest.

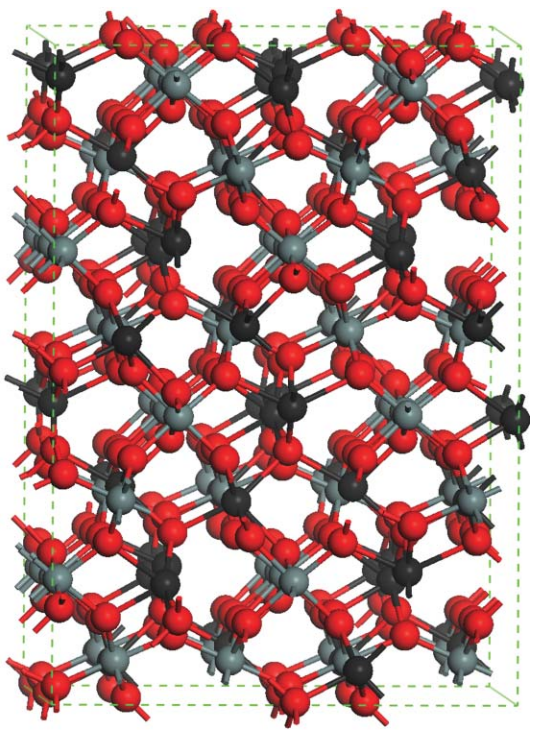

Fig. 1 The crystal structure of α-$Bi_2Sn_2O_7$. There are 32 formula units and 352 atoms in the unit cell. The O atoms are coloured red, the Sn atoms are grey and the Bi atoms black.

[a]*School of Chemistry, University Of Dublin, Trinity College, Dublin 2, Ireland. E-mail: watsong@tcd.ie*
[b]*Department of Chemistry, Inorganic Chemistry Laboratory, South Parks road, Oxford, UK OX1 3QR*

Experimentally a number of structural studies by diffraction techniques have been made[7,16] and there has also been extensive investigation of catalytic activity.[1,2] However, no photoemission experiments on $Bi_2Sn_2O_7$ have been performed to date. Additionally, due to the large size of the unit cell no calculations of the electronic structure have been undertaken. The mechanism of oxidation reactions on $Bi_2Sn_2O_7$ surfaces and the role of the Bi 6s lone pair in surface reactivity remain a matter of conjecture.

In this study we perform the first electronic structure study of α-$Bi_2Sn_2O_7$ from both a theoretical and an experimental approach. A combination of both a rigorous *ab initio* method and X-ray photoemission spectroscopy is used to investigate the valence band density of states and shed light on the underlying interactions in this material. The results will contribute to the understanding of Bi(III) based pyrochlores in addition to opening up possibilities for the design of new materials.

2. Methods

a Computational

Density functional theory (DFT) as embodied in the Vienna *Ab-initio* Simulation Package[17–19] was used to calculate the electronic structure of α-$Bi_2Sn_2O_7$. The Kohn–Sham equations[20] were solved self consistently using the blocked Davidson diagonalization routine. The forces on the atoms were calculated using the Hellman–Feynman theorem and the atoms relaxed until the forces had converged to less than 0.01 eV $Å^{-1}$ and the pressure on the cell had equalized (constant volume). Gradient corrections were applied to the exchange-function using the implementation of Perdew, Burke and Ernzerhof.[21]

The wavefunctions were represented in terms of a plane wave basis set, with periodic boundary conditions applied in all three directions to approximate a bulk solid. The projector augmented wave method[22] (PAW) was used to represent the interaction between the core electrons (Bi, Sn: [Xe], O: [He]) and the valence electrons, as it approaches the accuracy of an all electron calculation while maintaining the computational efficiency of the pseudopotential approach by reducing the number of plane waves required. The fixed core states were generated from all-electron scalar relativistic calculations and as such the kinematic relativistic effects are included while the spin–orbit coupling is averaged. The plane wave cutoff energy and *k*-point density, obtained using the Monkhorst–Pack[23] method, were both checked for convergence for each system to be within 0.01 eV per Bi. Following a series of test calculations a plane wave cutoff of 500 eV was used and a *k*-point grid density of 4 × 4 × 4 was employed, resulting in a total number of 16 irreducible *k*-points.

b Experimental

Polycrystalline $Bi_2Sn_2O_7$ was prepared by the solid state reaction between stoichiometric quantities of Bi_2O_3 and SnO_2 at 1100 °C. The X-ray powder pattern of the resulting product was identical to that of the room temperature α phase reported in a recent variable temperature study.[6] The powder material was pressed into 13 mm diameter discs between tungsten carbide dies at 10 tons loading and then sintered at 1100 °C to give strong ceramic discs.

High-resolution X-ray photoemission spectra were measured in a Scienta ESCA 300 spectrometer. This incorporates a rotating anode Al Kα ($h\nu$ = 1486.6 eV) X-ray source, a 7 crystal X-ray monochromator and a 300 mm mean radius spherical sector electron energy analyser with parallel electron detection system. The X-ray source was run with 200 mA emission current and 14 kV anode bias, with the analyser operated at 150 eV pass energy with 0.8 mm slits. Gaussian convolution of the analyser resolution with a linewidth of 260 meV for the X-ray source gives an effective instrument resolution of 350 meV. As-presented samples displayed an O 1s line free of high binding energy structure due to carbonate or hydroxide contamination and a relatively weak C 1s peak due to hydrocarbon contamination. The intensity of this peak relative to the O 1s peak was reduced to about 1/40 by annealing at 300 °C. Annealing at higher temperature by rear face electron beam heating led to almost complete elimination of the C 1s peak, but at the expense of a radical reduction in the intensity of the Bi 4f peak relative to that of the Sn 3d peaks. Thus we present the former data. Sample charging was extremely problematic and it was necessary to stabilise the surface charge with an electron flood gun delivering 10 eV electrons. Binding energies were referenced to the residual C 1s peak, which was assigned a binding energy of 285.0 eV.

3. Results

a Calculated electronic structure

Structural optimizations at a series of volumes were performed, allowing the atomic positions, the lattice vectors and angles to relax within a constrained total volume. The resulting energy *versus* volume curve was fitted to the Murnaghan equation of state[24] to obtain the equilibrium cell volume, Fig. 2. Structural optimization of α-$Bi_2Sn_2O_7$ yielded the cell parameters shown in Table 1. The initial forces beginning from the experimental structure[6] were quite small with the largest forces being on the O ions. The relaxed structure maintained

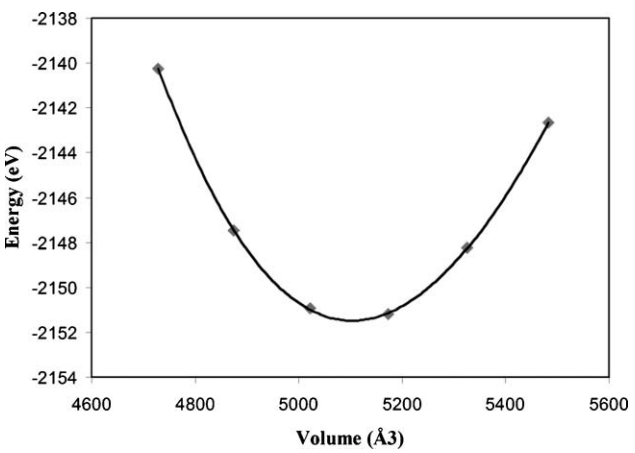

Fig. 2 Data from the volume optimization of $Bi_2Sn_2O_7$ fitted to the Murnaghan equation of state.

Table 1 Calculated binding energy and structural data for $Bi_2Sn_2O_7$ and percentage error with respect to experimental data[6]

Energy/eV per Bi	−33.62
Volume/Å^3	5118.46
a/Å	15.34 (+1.9%)
b/Å	15.34 (+1.9%)
c/Å	21.74 (+1.1%)

the almost tetragonal symmetry of the monoclinic unit cell, with $\beta = 90.043^\circ$. The calculated lattice vectors are within 1.9% of the experimentally determined values. The Bi atoms are five coordinate with respect to O and have Bi–O nearest neighbour distances averaging from 2.3 to 2.5 Å. The Sn atoms are six coordinate with respect to oxygen and have Sn–O nearest neighbour distances ranging from 2.0 Å to 2.2 Å. Both the Bi and Sn coordination data are in good agreement with the X-ray diffraction data.[3] For comparison with the thermodynamically stable α phase we also performed an additional structural optimization of $Bi_2Sn_2O_7$ in the regular cubic pyrochlore structure. The resulting binding energy was 0.27 eV per Bi atom higher than the distorted structure, confirming that the latter is energetically favoured, as expected.

The electron density for the valence states (between −12 eV and 0 eV) is shown for a slice through the unit cell containing both Bi and Sn atoms within the 010 plane in Fig. 3. The states below −12 eV (Bi 5d and O 2s) were excluded and they do significantly contribute to the bonding and serve to obscure the remaining electron density. Through this plane the electron densities of the Sn–O chains and the Bi–O chains are clearly separated, with two rows of each layer present in the unit cell. The bottom row contains both Bi and O atoms. The oxygen atoms contain near spherical regions of high electron density, representative of their almost complete 2p shell (based on a formal oxidation state of −2). Each Bi is coordinated by two O atoms in the 010 plane and an additional three oxygens out of the plane. This five fold coordination is similar to that found in the thermodynamically stable phase of Bi_2O_3. The electron density around each Bi atom is distorted toward the direction pointing away from the coordinated O atoms and thus provides evidence of a weakly directional lone pair. The second row from the bottom of the unit cell contains both Sn and O atoms. The density around the O atoms is similar in both size and shape to the Bi–O row, while the density around Sn is much weaker in comparison to Bi. This low region of electron density around the Sn atoms is quite representative of the +4 state ascribed to Sn, where the majority of the 5s and 5p electrons have been lost to O.

The total electronic density of states (EDOS) is shown in Fig. 4(a). Six main regions can be identified below the Fermi level, and a bandgap of 1.98 eV between the valence and conduction bands is observed. The partial (*l* and *m* quantum number decomposed) electronic density of states (PEDOS) has also been calculated for each ionic species. These were obtained by projecting the wavefunctions onto spherical harmonics centred on each atom with a radius of 1.65 Å for Bi, 1.60 Å for Sn and 1.55 Å for O. These radii were checked to

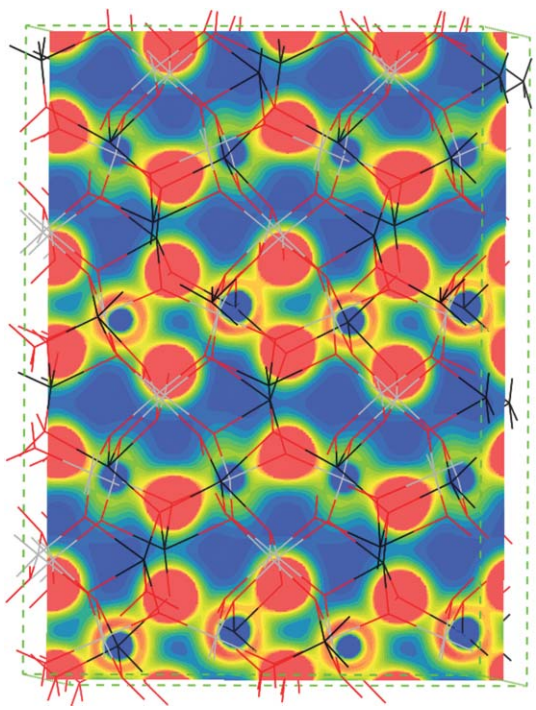

Fig. 3 An electron density map for the valence states in $Bi_2Sn_2O_7$, plotted through the 010 plane from 0 (blue) to 0.4 e Å^{-1} (red). The O atoms are coloured red, the Sn atoms are grey and the Bi atoms black.

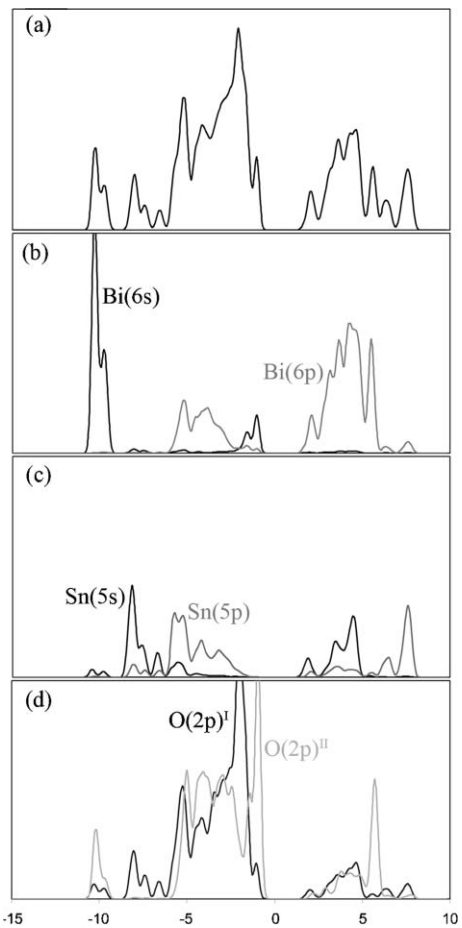

Fig. 4 The electronic density of states (EDOS) of $Bi_2Sn_2O_7$. (a) Total EDOS, (b) Bi partial EDOS, (c) Sn partial EDOS and (d) O partial EDOS for two types of oxygen ion.

ensure reasonable space filling and that they give rise to the correct number of electrons. The results (at least the qualitative aspects) are insensitive to changes in the radii.

The PEDOS for Bi is shown in Fig. 4(b). The majority of occupied Bi states are located at the bottom of the valence band, with a large Bi 6s peak at −10 eV. A Bi 6p peak is present between −5 eV and −1 eV, with a small Bi 6s peak present just below the Fermi level. The conduction band is dominated by Bi 6p states. The lowest energy states found in the Sn PEDOS are also s based, with a Sn 5s peak present between −9 eV and −5 eV, Fig. 4(c). A peak consisting of Sn 5p states runs from −5 eV to the top of the valence band. In the case of Sn the bottom of the conduction band is dominated by states derived from Sn 5s.

Oxygen atoms with two types of coordination can be found which result in two different PEDOS as shown in Fig. 4(d). Type I oxygen is coordinated to two Sn atoms and one Bi atom, while type II oxygen is coordinated to three Bi atoms. The PEDOS for type II oxygen shows a clear O 2p peak overlapping with the Bi 6s peak at the bottom of the valence band. O 2p states are present between −5 eV and −1 eV overlapping with the Bi 6p states. An additional peak is found at the top of the valence band overlapping with the high energy Bi 6s peak. The PEDOS derived for type I oxygen shows more overlap with the Sn states as would be expected. The peak at −10 eV is diminished, with O 2p states now present between −9 eV and −6 eV overlapping with Sn 5s. The O 2p peak at the top of the valence band is also reduced.

The states at the top of the valence band will of course be important in any reactivity. The PEDOS shows that the top of the valence band is dominated by a mixture of Bi 6s and O 2p states. This can also be observed in the electron density arising from states between −2 eV and 0 eV, Fig. 5. The electron density map also confirms that the asymmetry in the electron density of Bi results from states at the top of the valence band, and not from the main Bi 6s peak at −10 eV. This, and the lack of electron density between the Bi and O atoms, are both in line with the concept that the ns^2 lone pairs in heavy metal ceramics arise from the antibonding combination between the metal s and anion p states, which subsequently mix with metal p states in an asymmetric environment, producing the observed distortion in the electron density.[9,10] It is the interaction of oxygen which mediates the mixing of Bi 6s and 6p. The Sn atoms contribute almost no electron density to the top of the valence band. Sn undergoes similar interactions with O to those of Bi, but in the case of Sn(IV) the antibonding metal s–anion p states are unfilled.

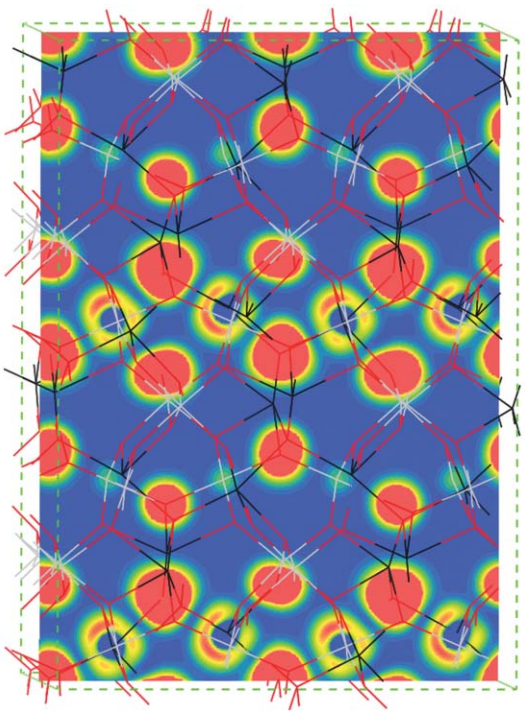

Fig. 5 A partial electron density map for the states between −2 eV and 0 eV, with reference to the Fermi level, in $Bi_2Sn_2O_7$, plotted through the 010 plane from 0 (blue) to 0.15 e $Å^{-1}$ (red). The O atoms are coloured red, the Sn atoms are grey and the Bi atoms black.

b X-Ray photoemission data

The principal core level peaks—Bi 4f, Sn 3d and O 1s—are shown in Fig. 6 and the core level binding energies, halfwidths and intensities are summarised in Table 2. The Sn 3d core lines

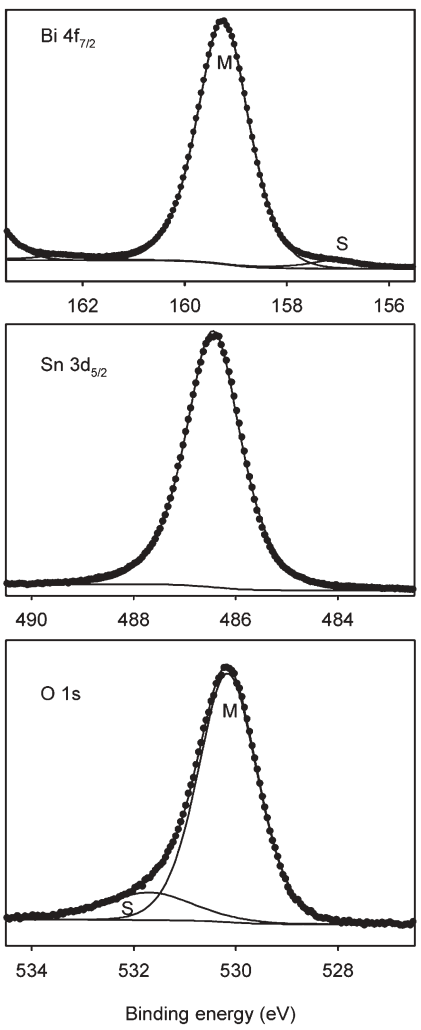

Fig. 6 The principal core lines in XPS of $Bi_2Sn_2O_7$.

Table 2 Core level binding energies, FWHM values and intensities for $Bi_2Sn_2O_7$.

	Bi $4f_{7/2}$	Sn $3d_{5/2}$	O 1s
Binding energy/eV	159.25 M	486.44	530.15 M
	157.06 S		531.70 S
Relative intensity	1.92 M		5.44 M
	0.10 S		1.09 S
	2.02 T	1.98	6.53 T
FWHM/eV	1.19 M	1.27	1.37 M
	1.20 S		2.04 S

[a] For the Bi 4f and O 1s data, M, S and T refer respectively to the main peak, shoulder and total. Relative intensities have been corrected by atomic sensitivity factors.

can be fitted with a pair of simple Voigt functions for the spin orbit doublet with a Sn $3d_{5/2}$ binding energy of 486.44 eV. This is quite close to the value of 487.00 eV found for SnO_2.[25] The Bi 4f core structure is dominated by $4f_{7/2}$ and $4f_{5/2}$ components at 159.25 eV and 155.08 eV. However there are also a pair of weak but well-defined components shifted by 2.19 eV to lower binding energy of the main core lines and giving rise to distinct low energy shoulders. The Bi $4f_{7/2}$ binding energy of this component is at 157.06 eV, intermediate between the values for Bi metal (156.85 eV) and typical Bi(III) oxides (159.0 eV to 159.8 eV).[26] The low binding energy peaks are tentatively attributed to Bi(I) species in the near surface region. Finally the O 1s peak fits to a component at 530.15 eV and a second component with about 1/6 the intensity of the first at 531.70 eV. The shift between the two components of 1.55 eV is less than shifts in excess of 2 eV typically found between intrinsic core lines in oxides and core peaks associated with hydroxide or carbonate surface contamination. It is therefore tempting to associate the two peaks with the two very different oxygen sites (usually designated as O and O′) found in the pyrochlore structure, although this conclusion cannot be regarded as definitive. The surface stoichiometry inferred from normalisation of the core level intensities with atomic sensitivity factors[25] is $Bi_{1.98}Sn_{2.02}O_{6.53}$. The small deviation of the oxygen stoichiometry from its ideal value is consistent with oxygen loss in the near surface region and the apparent presence of surface Bi(I) species.

The valence band XPS is shown in Fig. 7 along with the calculated density of states. There is a very good correspondence between the theoretical density of states and the experimental spectrum. In particular six components labelled I–VI can be identified in each. The two bands V and VI which are found at the bottom of the valence band correspond to the bonding Sn 5s and Bi 6s states, both of which are hybridised to some extent with the O 2p states. The next three bands II, III and IV correspond to the main O 2p valence band state, which hybridise mainly with Sn 5p and Bi 6p states to give M–O bonding states. The extent of hybridisation is most pronounced in the relatively sharp band IV. Finally the relatively weak band I which appears in the experimental spectrum as a well defined shoulder at the top of the valence band, corresponds to the Bi 6s–O 2p antibonding levels, which in turn hybridise with Bi 6p states to give the asymmetric electron density discussed above. The only major discrepancy between

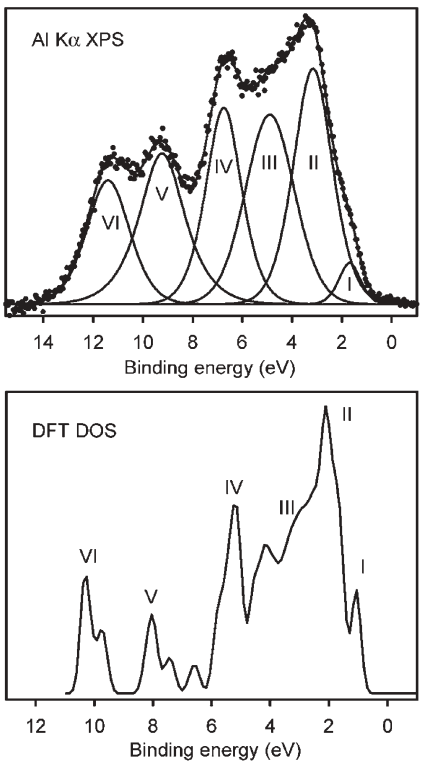

Fig. 7 Comparison between valence band XPS of $Bi_2Sn_2O_7$ and the density of states from DFT calculations. Note that the overall spread of energies in the experimental spectrum is 16.5 eV and only 14 eV in the calculated DOS. A Shirley background has been subtracted from the experimental spectrum.

the experimental and theoretical data is that the overall spread of energies is greater in the former. This is a general problem when comparing densities of states from DFT calculations with experimental data.[27] The close correspondence between the calculated *total* density of states and the experimental photoemission spectrum suggest that cross sections for ionisation of O 2p, Sn 5s and 5p and Bi 6s and 6p states are all rather similar. This is not quite in accord with the calculated ionisation cross sections of Yeh and Lindau[28] which would give much greater spectral weight to the metal s and p states than to the O 2p states. This discrepancy has been noted before in comparing X-ray photoemission data for PbO_2,[29] PbO and Bi_2O_3[15] with theoretical densities of states and suggests that the calculated cross sections are not entirely reliable. This is perhaps a reflection of the fact that the shapes of valence s and p orbitals of heavy elements in the core region are strongly influenced by relativistic effects that are not treated in the cross section calculations.

4. Discussion

Both the theoretical density of states and the experimental XPS spectra indicate a high degree of covalency in the system. Bader analysis[30] of the calculated charge density results in electron populations of 13.10 and 12.53 for Bi and Sn respectively. The effective oxidation states of approximately +2.0 for Bi and +1.5 for Sn clearly deviate from the idealised

Bi(III) and Sn(IV) species. The PEDOS shows that bonding interactions occur between oxygen and the valence s states of both Sn and Bi. The main difference between the metal–oxygen interactions lies in the fact that for Bi the antibonding combination of this interaction is filled, while for Sn the antibonding combination lies above the Fermi level.

$Bi_2Sn_2O_7$ exhibits a number of unique properties relative to other Sn based pyrochlores involving the oxidation of various organic species and gas sensing with selectivity for CO. Key to all these processes is the reduction of the Sn atoms. What is unclear is why $Bi_2Sn_2O_7$ exhibits oxidizing properties exceeding those of the similar materials. Replacing Bi with like sized metals results in the formation of the symmetric regular pyrochlore lattice. This can be ascribed to the asymmetric electron density of Bi(III) distorting the crystal lattice. A distorted environment allows for coupling between the Bi 6s and 6p states and the filled antibonding states are stabilized. As such the formation of the lone pair (and hence distorted) structure is favoured. A recent DFT study by Pruneda and Artacho[31] addressed a series of $A_2B_2O_7$ compounds which adopt the regular cubic pyrochlore lattice. Replacing Bi with La or Y removes the strong overlap with the valence O 2p states which we observe for $Bi_2Sn_2O_7$.

Sn in its +2 oxidation state, much like Bi(III), is known to form an asymmetric electron density and have a strong preference for distorted structures.[10] In an oxidative catalytic process the reduction of Sn(IV) will produce a Sn(II) species. A donation of electrons to Sn in $Bi_2Sn_2O_7$ will fill the antibonding Sn 5s–O 2p orbitals. Similar to Bi, a distorted coordination environment will allow for the additional bonding interaction of the metal p states with the antibonding orbitals, thus making the reduced configuration more energetically stable. This emerging hypothesis is much akin to the reason why SnO adopts the distorted litharge structure as apposed to cubic rocksalt.[10] The Bi–O layers in this pyrochlore create a distorted structural backbone for Sn–O layers which will make reduction of the Sn atoms more energetically favorable than it would be in a regular cubic pyrochlore lattice. This would explain why the inclusion of Bi in this pyrochlore aids the catalytic activity of the material. While the large size of the unit cell is computationally restricting, it would be of significant interest for future studies to address the reduction of a Sn terminated surface of α-$Bi_2Sn_2O_7$ in comparison to the regular pyrochlore lattice and other pyrochlore structures.

5. Conclusions

The electronic structure of the pyrochlore bismuth stannate, $Bi_2Sn_2O_7$, has been calculated using gradient corrected density functional theory and examined experimentally using X-ray excited valence band photoemission spectroscopy. A full ionic relaxation was performed in the calculations and the resulting structure is in good agreement with experiment. The features of the calculated density of states and the XPS spectra are in excellent agreement and both indicate a high degree of covalency in the system. Strong interactions occur between oxygen and both Sn and Bi. The orbital populations support formation of this oxide as $Bi(III)_2Sn(IV)_2O_7$ but the compound is highly covalent with Bader charges of +1.9 and +1.47 on Bi and Sn respectively. A mixture of Bi 6s and O 2p states are found to dominate the top of the valence band while Sn 5s, O 2p and Bi 6p states dominate the bottom of the conduction band. This is due to differences in the strengths of the metal s interactions with O 2p. The maxima in the occupied Bi 6s and Sn 5s partial densities of states are found at the bottom of the valence band and the Bi 6s contribution at the top of the valence band arises only because of the covalent interactions with O 2p states. It is proposed that it is the distorted coordination environment produced by the Bi–O layers which aids the reduction of Sn(IV) to Sn(II) and as such enhances the catalytic activity of this material.

Acknowledgements

We would like to acknowledge the HEA for a PRTLI (Cycle III) grant and the University of Dublin for a Trinity College Postgraduate Studentship. All calculations were performed on the IITAC cluster maintained by TCHPC. The NCESS facility at Daresbury Laboratory is supported by EPSRC.

References

1 C. A. Mims, A. J. Jacobson, R. B. Hall and J. T. Lewandowski, *J. Catal.*, 1995, **153**, 197.
2 L. Moens, P. Ruiz, B. Delmon and M. Devillers, *Catal. Lett.*, 1997, **46**, 93.
3 G. S. V. Coles, S. E. Bond and G. Williams, *J. Mater. Chem.*, 1994, **4**, 23.
4 G. S. Devi, S. V. Manorama and V. J. Rao, *J. Electrochem. Soc.*, 1998, **145**, 1039.
5 R. D. Shannon, J. D. Bierlein, J. L. Gillson, G. A. Jones and A. W. Sleight, *J. Phys. Chem. Solids*, 1980, **41**, 117.
6 I. R. Evans, J. A. K. Howard and J. S. O. Evans, *J. Mater. Chem.*, 2003, **13**, 2098.
7 Ismunadar, B. J. Kennedy, B. A. Hunter and T. Vogt, *J. Solid State Chem.*, 1997, **131**, 317.
8 G. W. Watson and S. C. Parker, *J. Phys. Chem. B*, 1999, **103**, 1258.
9 A. Walsh and G. W. Watson, *J. Solid State Chem.*, 2005, **178**, 1422.
10 A. Walsh and G. W. Watson, *Phys. Rev. B*, 2004, **70**, 235114.
11 A. Walsh and G. W. Watson, *J. Phys. Chem. B*, 2005, **109**, 16686.
12 P. Glans, T. Learmonth, C. McGuiness, K. Smith, J. Guo, A. Walsh, G. W. Watson and R. Egdell, *Phys. Rev. B*, 2005, **71**, 235109.
13 P. Glans, T. Learmonth, C. McGuiness, K. Smith, J. Guo, A. Walsh, G. W. Watson and R. Egdell, *Chem. Phys. Lett.*, 2004, **399**, 98.
14 D. J. Payne, R. G. Edgell, A. Walsh, G. W. Watson, J. Guo, P. A. Glans, T. Learmonth and K. E. Smith, *Phys. Rev. Lett.*, 2006, **96**, 157403.
15 A. Walsh, G. W. Watson, D. J. Payne, R. G. Edgell, J. Guo, P. A. Glans, T. Learmonth and K. E. Smith, *Phys. Rev. B*, 2006, **73**, 235104.
16 R. S. Jones and K. S. Knight, *J. Chem. Soc., Dalton Trans.*, 1997, **15**, 2551.
17 G. Kresse and J. Hafner, *Phys. Rev. B*, 1994, **49**, 14251.
18 G. Kresse and J. Furthmuller, *Comput. Mater. Sci.*, 1996, **6**, 15.
19 G. Kresse and J. Furthmuller, *Phys. Rev. B*, 1996, **54**, 11169.
20 W. Kohn and L. J. Sham, *Phys. Rev.*, 1965, **140**, A1133.
21 J. P. Perdew, K. Burke and M. Ernzerhof, *Phys. Rev. Lett.*, 1996, **77**, 3865.
22 P. E. Blöchl, *Phys. Rev. B*, 1994, **50**, 17953.
23 H. J. Monkhorst and J. D. Pack, *Phys. Rev. B*, 1976, **13**, 5188.
24 F. D. Murnaghan, *Proc. Natl. Acad. Sci. U. S. A.*, 1944, **30**, 244.
25 R. G. Egdell, J. Rebane, T. J. Walker and D. S. L. Law, *Phys. Rev. B*, 1999, **59**, 1792.

26 *Practical Surface Analysis*, ed. D. Briggs and M. P. Seah, Wiley, Chichester, 1994.
27 Y. Dou, R. G. Egdell, D. S. L. Law, N. M. Harrison and B. G. Searle, *J. Phys.: Condens. Matter*, 1998, **10**, 8447.
28 J. J. Yeh and I. Lindau, *At. Data Nucl. Data Tables*, 1985, **32**, 1.
29 D. J. Payne, R. G. Egdell, W. Hao, J. S. Foord, A. Walsh and G. W. Watson, *Chem. Phys. Lett.*, 2005, **411**, 181.
30 R. Bader, *Atoms in Molecules: A Quantum Theory*, Oxford University Press, New York, 1990.
31 J. M. Pruneda and E. Artacho, *Phys. Rev. B*, 2005, **72**, 085107.

